Structure and dynamics of the liquid 3d transition metals near melting. An *ab-initio* study

Beatriz G del Rio, Carlos Pascual, Luis E González and David J González

Departamento de Física Teórica, Universidad de Valladolid, Valladolid, SPAIN

E-mail: `david@metodos.fam.cie.uva.es`

Abstract. The static and dynamic properties of several bulk liquid $3d$ transition metals at thermodynamic conditions near their respective melting points have been evaluated by using *ab-initio* molecular dynamics simulations. The calculated static structure factors, show an asymmetric second peak followed by a more or less marked shoulder which points to a sizeable amount of icosahedral local order. Special attention is devoted to the analysis of the longitudinal and transverse current spectral functions and the corresponding dispersion of collective excitations. For some metals, we have found the existence of two branches of transverse collective excitations in the second pseudo-Brillouin zone. Finally, results are also reported for several transport coefficients.

Submitted to: *J. Phys.: Condens. Matter*

1. Introduction

The transition metals and their alloys are materials with great technological interest because of their wide range of applications. This fact underlies the importance of the research concerning a better undertanding of their structural and dynamical properties.

This paper reports an *ab-initio* molecular dynamics simulation study of several structural and dynamical properties of some bulk liquid $3d$ transition metals at thermodynamic conditions near melting. The present study completes previous calculations for liquid Ti (l-Ti), l-Fe and l-Ni [1, 2, 3], which we have now extended to l-Sc, l-V, l-Cr, l-Mn and l-Co. Oddly enough, the practical relevance of these transition metals has not been matched by a wealth of experimental data for their static and dynamic properties in the liquid state.

Information about the structural short-range order in a liquid system can be extracted from the static structure factor, $S(q)$. For the above mentioned $3d$ transition metals, their respective $S(q)$ was first measured by X-ray diffraction (XD) experiments carried out by Waseda and coworkers (WC) [4] more than forty years ago. Since then, only the $S(q)$ of l-Ti, l-Fe and l-Ni have been determined again by either XD or neutron diffraction (ND) experiments [5, 6] leading in some cases, i.e. l-Ti, to new results in qualitative disagreement with WC's XD (WCXD) data [4]. Those discrepancies underlie, in our opinion, the need for new measurements of the $S(q)$ for the other $3d$ transition metals, and this fact has prompted us to perform the present *ab-initio* simulations.

As for the dynamical properties, data for several transport coefficients, have already been reported for most of the 3d metals [8, 9, 10, 11]. In the case of l-Ti, l-Fe and l-Ni near melting, the corresponding dynamical structure factors have been measured by both inelastic X-ray and neutron scattering [12, 13, 14]. However, we are not aware of similar experimental measurements for the other $3d$ transition metals.

Quite a few theoretical studies, either based on semiempirical or more fundamental methods, have already been devoted to the study of the liquid $3d$ transition metals and they have mainly focused on thermodynamic or static structural properties. Among those, we mention the early semiempirical study of Todd and Brown [15], which basically used the hard

spheres model to obtain a reasonable estimate of the $S(q)$. Haustleitner *et al* [16] studied the static structure of several liquid transition metals by means of an effective interionic pair potential which was used together with classical Molecular Dynamics (CMD) simulations and liquid state theories. A similar approach was followed by Bhuiyan *et al* [17] who used a variational theory of liquids [18] to compute the static structure factors, free energies and entropies of several liquid $3d$, $4d$, and $5d$ transition metals.

Our previous study of l-Ti, l-Fe and l-Ni devoted particular attention to the investigation of their collective dynamic properties. This was prompted by the recent finding [19, 20, 21] of some unusual dynamical features such as transverse low-energy excitations in the dynamic strucure factor and/or the appearance of a second, high-frequency peak, in the transverse current spectral functions. Still, we lack an understanding of the dynamical processes behind the emergence of the those features. Nevertheless, we have recently found some connection between the appearance of the second peak in the transverse spectral function and the coupling of the transverse current with density fluctuations at all wavevectors [22].

The paper has been structured as follows: the next section contains some basic information on the AIMD simulation method. Section 3 reports the results of the calculations which are compared with the available experimental data along with some discussion. Finally, in section 4 we summarize the conclusions of this study.

2. Computational method

This study has been carried out for the metals and thermodynamic states specified in Table 1. The number of atoms used in the simulations varied from 100 atoms (l-Cr) to 135 atoms (l-Co) located in a cubic supercell.

The AIMD simulations were performed with the Quantum-ESPRESSO package [23], which is based on density functional theory [24]. The electronic exchange-correlation energy has been described by the generalized gradient approximation of Perdew-Burke-Ernzerhof [25], including non-linear core corrections. The ion-electron interaction has been taken into accounted by an ultrasoft pseudopotential [26], which was generated from a scalar-relativistic calculation.

For all systems, the initial atomic positions within

Table 1. Thermodynamic input data of the liquid 3d transition metals studied in the present AIMD simulation study. ρ is the total ionic number density, taken from Ref. [17]. T is the temperature, N_{part} the number of particles used in the simulation, Δt the timestep and N_c the total number of configurations.

	ρ (Å^{-3})	T(K)	N_{part}	Δt (ps)	N_c
Sc	0.0391	1875	120	0.0045	29000
V	0.0634	2173	120	0.0040	20000
Cr	0.0713	2173	100	0.0045	27000
Mn	0.0655	1550	120	0.0045	13200
Co	0.0787	1850	135	0.0045	13100

the cell were taken at random and the system was thermalized during $5 - 10$ ps of simulation time; therefrom, microcanonical AIMD simulations were performed over a number of time steps as given in Table 1. We applied a plane-wave representation with an energy cutoff within the range 25.0 - 35.0 Ryd and the single Γ point was used for sampling the Brillouin zone. Finally, we remark that the number of equilibrium configurations listed in Table 1 were those employed for the evaluation of the static and dynamic properties of the corresponding liquid metal. This same simulation method has already provided an accurate description of several static, dynamic and transport properties of other bulk liquid metals [1, 2, 3, 27].

3. Results and discussion

3.1. Static properties

The obtained results for the respective $S(q)$ are plotted in Figures 1-2 where we have also depicted the corresponding WCXD data [4]. In the case of l-Ti, l-Fe and l-Ni we have also included the more recent XD and ND experimental data [5, 6]. For these metals, the excellent agreement of the AIMD simulations with the more recent experimental data provides, in our opinion, additional confidence on the AIMD results obtained for the other $3d$ transition metals.

Excepting l-Sc and l-Ti, there is an overall qualitative agreement between the present AIMD results and the WCXD data. Some minor discrepancies are apparent, such as: (i) a small phase shift in l-V, l-Mn and l-Co and (ii) differences in the shape of the second peak, as the present AIMD results predict an asymmetric second peak followed by a more or less marked shoulder, whereas the XD data show for all systems a symmetric second peak. Nevertheless, it is worth mentioning that an asymmetric shape of the second peak with a shoulder on its high-q side has been found in several liquid metals, including l-Ti, l-Ni and l-Zr [5, 6, 7], and it has been related to the appearance of a sizeable amount of icosahedral (ICOS) local order.

We already mentioned that the calculated $S(q)$ for
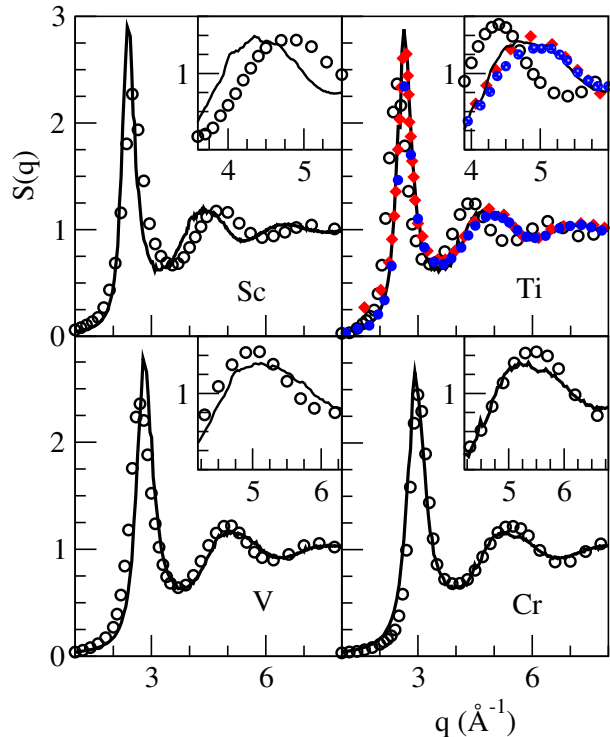
Figure 1. Static structure factor, $S(q)$, of l-Sc, l-Ti, l-V and l-Cr. Continuous line: present AIMD calculations. Open circles: WCXD data from [4]. The blue and red circles in l-Ti represent the XD and ND data [6] respectively. The inset shows a detailed comparison for the second maximum.

l-Sc and l-Ti showed a strong dephasage in comparison with WCXD data. Nevertheless, a comparison with the more recent XD and ND data [6] for l-Ti, revealed a similar shift of ≈ 0.20 Å^{-1} with respect to WCXD data. Furthermore, the more recent XD data [6] displayed a second peak with a clear shoulder on the high-q side. Taking into account the above inaccuracies of WCXD data for l-Ti, we think that something similar might happen for l-Sc, where an analogous (although opposite) dephasage is visible when compared with the present AIMD result.

A useful method of describing the short range order in liquid metals was suggested by Honeycutt and Andersen [28]. We have used a simplified version which identifies the number and properties of the atoms surrounding a pair of near-neighbors. This is achieved by assigning a set of four indices to each bond. The first index is 1 if the root pair belongs to the first peak of $g(r)$, that is, their separation is smaller than the position of the first minimum of $g(r)$. The second index is the number of common first-neighbor atoms, the third index gives the number of near-neighbor bonds that connect those shared first neighbors and the fourth index is used to diferenciate among configurations with the same first three indices
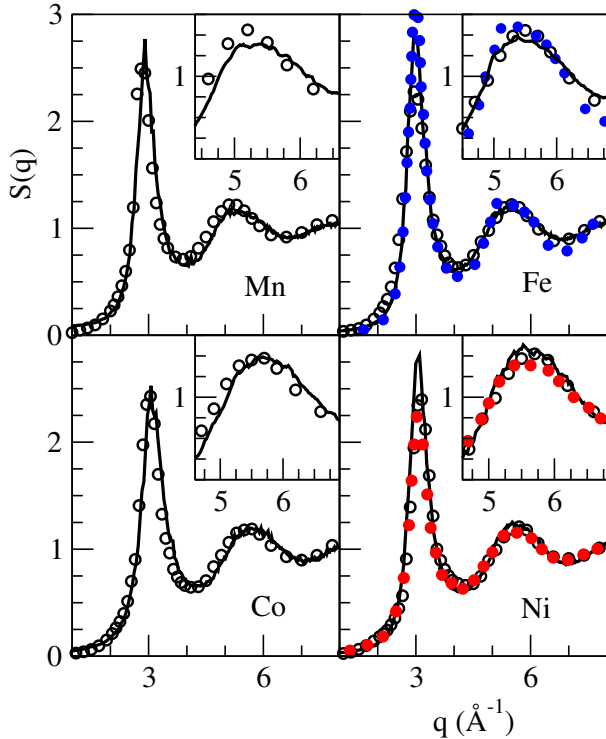
Figure 2. Same as the previous graph but for l-Mn, l-Fe, l-Co and l-Ni. The blue circles in l-Fe are XD data and the red ones in l-Ni are ND data [5]

Table 2. Honeycutt-Andersen pair fractions calculated from the AIMD configurations obtained for the liquid transition metals at the thermodynamic states given in Table 1. The results are compared with several local structures.

Pairs	1551	1541	1431	1421	1422	1441	1661
l-Sc	0.40	0.12	0.07	0.00	0.01	0.11	0.18
l-V	0.45	0.14	0.10	0.01	0.01	0.09	0.15
l-Cr	0.41	0.18	0.13	0.02	0.03	0.08	0.15
l-Mn	0.28	0.17	0.21	0.03	0.05	0.06	0.08
l-Co	0.31	0.18	0.23	0.04	0.08	0.03	0.06
ICOS	1.0	0.0	0.0	0.0	0.0	0.0	0.0
HCP	0.0	0.0	0.0	0.50	0.50	0.0	0.0
FCC	0.0	0.0	0.0	1.0	0.0	0.0	0.0
BCC	0.0	0.0	0.0	0.0	0.0	0.43	0.57

but with a different topology. This method allows to distinguish among various local structures like FCC, HCP, BCC and ICOS environments. For example, 142x-type pairs are typical of closed closed packed structures (FCC and HCP). Likewise, 155x pairs are characteristic of perfect icosahedra whereas 154x and 143x pairs characterize distorted icosahedra. 144x and 166x pairs indicate BCC structures.

Starting from several configurations generated in the present AIMD simulation, we have first removed the thermal noise by finding the corresponding inherent structures. Then the Honeycutt-Andersen method was applied and the obtained results are summarized in Table 2, where we have reported the most abundant pairs. Notice that the five-fold symmetry dominates in all these metals because the sum of perfect and distorted ICOS structures ranges between $\approx 59\%$ (l-Sc) and $\approx 72\%$ (l-Cr, l-Co) of the pairs. There is also a significant amount of local BCC-type pairs which range from $\approx 29\%$ (l-Sc) to $\approx 10\%$ (l-Co) of the pairs. It is precisely in l-Co where the FCC and HCP-type pairs have a contribution of $\approx 12\%$ while they are practically negligible for the other metals. At this point, it is worth noting that Co melts from a FCC structure whereas all the other elements in Table 2 do so from a BCC structure. Other indicators of the local atomic arrangement, such as the bond angle

distribution, or the distribution of Steinhardt's bond orientational order parameters, also point qualitatively in the same direction of a prevalence of ICOS local structures.

We have used our calculated $S(q)$, within the range $q \leq 1.3$ Å^{-1}, to estimate the value of $S(0)$. We applied a least squares fit, $S(q) = s_0 + s_2 q^2$, and Figure 3 shows the AIMD results along with the corresponding fit. Now, by using the relation $S(0) = \rho k_B T \kappa_T$, where k_B is Boltzmann's constant, we have evaluated the associated isothermal compressibility, and the results are given in Table 3, where they are compared with the available experimental data.

3.2. Dynamic properties

We have evaluated several dynamic properties and the calculation of the associated time correlation functions has been made by taking time origins every five time steps. Notice that the wave-vector $\vec{q}$ dependence in some correlation functions is transformed into a dependence on $q \equiv | \vec{q} |$ only, because of the macroscopically isotropic behavior of the fluid.

3.2.1. Single particle dynamics

For the single particle dynamics, we have focused on the velocity autocorrelation function (VACF) of a tagged ion in the fluid, $Z(t)$, which in the present simulations has been calculated as

$$Z(t) = \langle \vec{v}_1(t) \cdot \vec{v}_1(0) \rangle / \langle v_1^2 \rangle \tag{1}$$

with $\vec{v}_1(t)$ being the velocity of a tagged ion in the fluid at time t and $\langle ... \rangle$ stands for the ensemble average.

The AIMD results for $Z(t)$ are plotted in figure 4 where we observe the typical backscattering behavior with a marked first minimum which is followed
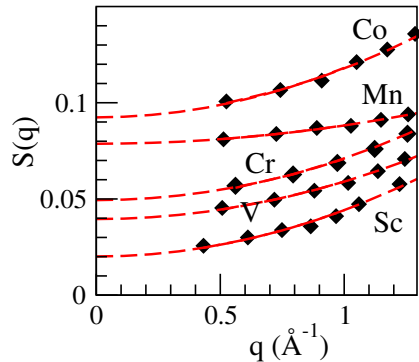
Figure 3. Small-q behavior of the AIMD calculated $S(q)$ (symbols). The dashed lines are the corresponding least squares fit mentioned in the text. The figures have been displaced vertically by 0.02 (V), 0.03 (Cr), 0.01 (Mn) and 0.07 (Co) units.

Table 3. Calculated values for $S(q \to 0)$ and isothermal compressibilities, κ_T, for the liquid transition metals at the thermodynamic states given in Table 1. The numbers in parenthesis are experimental and/or semiempirical data.

	$S(q \to 0)$	κ_T (10^{-11} m^2 N^{-1})
Sc	0.020 ± 0.002	2.00 ± 0.10 (3.25^a)
V	0.021 ± 0.002	1.10 ± 0.10 (1.43^a, 1.21^b)
Cr	0.020 ± 0.002	0.94 ± 0.10 (1.00^a, 1.10^b)
Mn	0.069 ± 0.003	4.9 ± 0.3 (3.00^a, 3.74 ± 0.02)
Co	0.022 ± 0.002	1.10 ± 0.10 (1.43^a, 1.18 ± 0.02^b)

[a] Ref. [29]
[b] Ref. [8]

by oscillations of decreasing amplitude. This first minimum is related to the so-called cage effect by which a given particle rebounds against the cage formed by its nearest neighbors. The inset in figure 4 represents the associated power spectrum, $Z(\omega)$, and we find that its shape may display a double peak (l-V and l-Co), a peak followed by a shoulder (l-Cr, l-Sc and l-Ni) or just one peak (l-Mn). We notice that in a recent ab-initio study of l-Tl [19], where the associated $Z(\omega)$ showed a peak followed by a marked shoulder, the authors pointed to some correlation between the appearance of a high frequency shoulder/peak and the emergence of a second high-frequency transverse branch with practically the same frequency as that of the peak/shoulder. We will analyze this point in the following section where the dispersion relation for the transverse current has been calculated.

The self-diffusion coefficient, D, can be calculated from the time integral of $Z(t)$ or from the slope, at very long times, of the mean square displacement $\delta R^2(t) \equiv \langle|\vec{R}_1(t) - \vec{R}_1(0)|^2\rangle$ of a tagged ion in the fluid, which are shown in figure 5. Both routes give practically the same results for D, which are reported in Table 4 with an uncertainty that reflects the two possibilities. To our
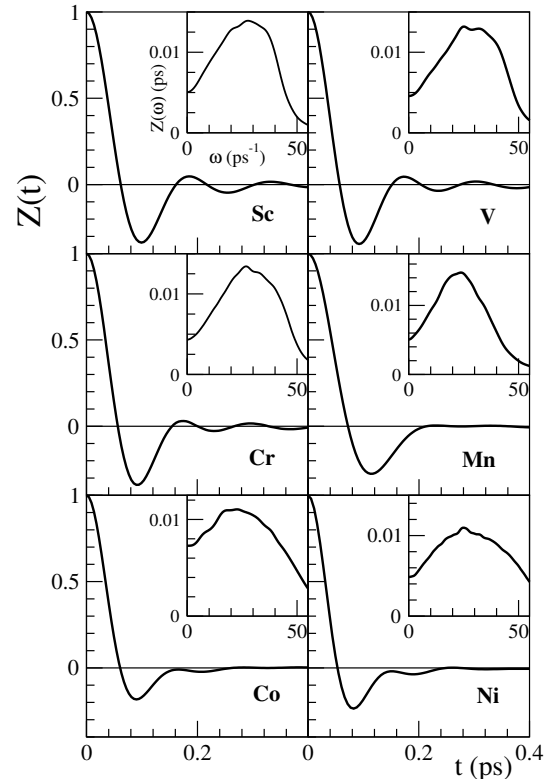
Figure 4. Normalized AIMD calculated velocity autocorrelation function of l-Sc, l-V, l-Cr, l-Mn, l-Co and l-Ni. The inset represents the corresponding power spectrum $Z(\omega)$.
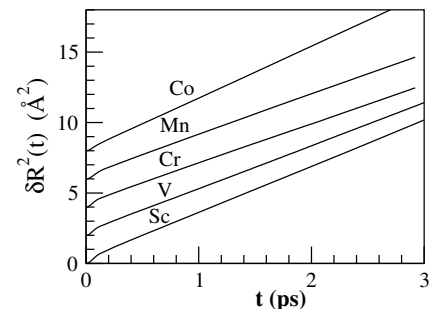
Figure 5. Calculated mean square displacements. The function corresponding to each element has been displaced vertically by 2 units consecutively.

knowledge, there are no experimental data to compare with; nevertheless, we stress that our previous AIMD study of l-Ti, l-Fe and l-Ni [1, 2, 3] yielded values in very good agreement with the respective experimental data.

3.2.2. Collective currents

We have evaluated the longitudinal, $J_L(q, t)$, and transverse, $J_T(q, t)$, current correlation functions from

Table 4. Calculated values of the self-diffusion coefficient(D), adiabatic sound velocity (c_s) and shear viscosity (η) for the liquid transition metals at the thermodynamic states given in Table 1. The numbers in parenthesis are experimental and/or semiempirical data.

	D (Å^2/ps)	c_s (m/s)	η (GPa ps)
Sc	0.55 ± 0.01	4400 ± 200	2.10 ± 0.10
V	0.51 ± 0.01	4725 ± 200 (4742[a])	3.30 ± 0.20
Cr	0.47 ± 0.01	4500 ± 200 (4298[a])	3.70 ± 0.20
Mn	0.46 ± 0.02	3100 ± 150 (3381[b])	2.50 ± 0.20
Co	0.60 ± 0.01	3700 ± 150 (4048[b])	3.20 ± 0.20
			(4.12[c], 3.60[d])

[a] Ref. [9]
[b] Ref. [8]
[c] Ref. [10]
[d] Ref. [11]

their definitions

$$J_L(q,t) = \frac{1}{N}\langle \vec{j}_L(q,t) \cdot \vec{j}_L^*(q,0)\rangle \tag{2}$$

$$J_T(q,t) = \frac{1}{2N}\langle \vec{j}_T(q,t) \cdot \vec{j}_T^*(q,0)\rangle \tag{3}$$

where $\vec{j}_L(q,t)$ and $\vec{j}_T(q,t)$ are the longitudinal and transverse components respectively of the microscopic current

$$\vec{j}(q,t) = \sum_{j=1}^{N} \vec{v}_j(t)\ \exp[i\vec{q}\cdot \vec{R}_j(t)]\,, \tag{4}$$

where N is the total number of particles and $\vec{R}_j(t)$ $\vec{v}_j(t)$ are the position and velocity of particle j at time t.

Using the configurations generated in the present AIMD simulations, we have used eqns. (2)-(4) to calculate the associated longitudinal and transverse currents, $J_L(q,t)$ and $J_T(q,t)$. Then, by numerical Fourier transform, we have obtained their respective spectra, $J_L(q,\omega)$ and $J_T(q,\omega)$, which have been calculated as a function of ω for a set of q-values within the range $0 \le q \le 2q_p$.

For each q-value, the obtained $J_L(q,\omega)$ show, for all metals, the same qualitative behavior, namely, it starts at zero for $\omega = 0$, then it increases towards a maximum value at a frequency $\omega_L(q)$ and finally it smoothly decays to zero for large frequencies. This can be observed in Figures 6-7 which represent, for several q-values, the obtained $J_L(q,\omega)$ for l-Sc and l-Co, as a function of ω.

From the position of the maxima, $\omega_L(q)$, in the function $J_L(q,\omega)$ we have derived the longitudinal dispersion relation for the associated collective modes. This has been plotted in Figure 8 where we observe the typical behaviour found in other liquid systems [30], with a maximum at $\approx q_p/2$ followed by a minimum located at $\approx q_p$. Moreover in the long
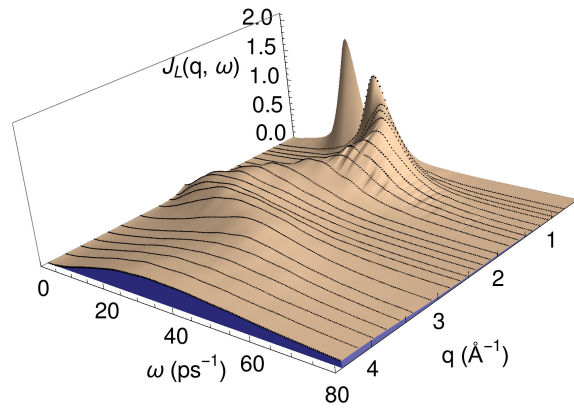
Figure 6. Longitudinal current spectra, $J_L(q,\omega)$, at several q-values for l-Sc at $T = 1875$ K.
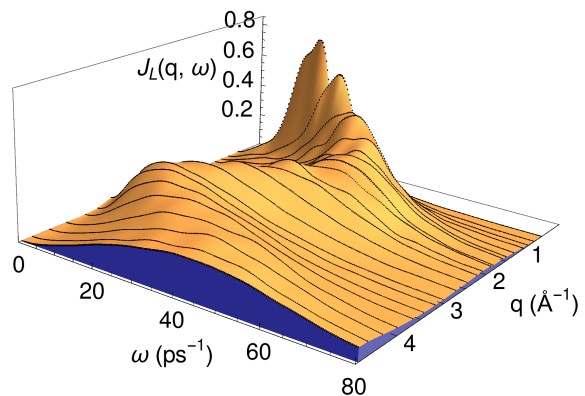
Figure 7. Same as before but for l-Co at $T = 1850$ K.

wavelength region, its slope gives a q-dependent adiabatic sound velocity $c_s(q) = \omega_L(q)/q$, which in the limit $q \to 0$ reduces to the bulk adiabatic sound velocity, c_s. Although we acknowledge that the smallest q-values attained in the present AIMD simulations are not very small because of the size of the simulation box, and they are already outside the hydrodynamic region, nevertheless we have calculated some qualitative estimates of c_s. Taking into account that the smallest q-values range from $q_{min} = 0.43$ Å^{-1} (Sc) to $q_{min} = 0.56$ Å^{-1} (Cr), we have extrapolated from the values $c_s \approx \omega_L(q_{min})/q_{min}$ and the results are given in Table 4. Despite the previous limitations, the calculated values show a reasonable agreement with the available semiempirical [8] and/or experimental [9, 11] data.

$J_T(q,t)$ provides information on the shear modes, and its spectrum, $J_T(q,\omega)$, when plotted as a function of ω, may display peaks within some q-range, which are related to propagating shear waves. We have found that, for all systems, the corresponding $J_T(q,\omega)$ already showed a peak at the q_{min}, then as q increases
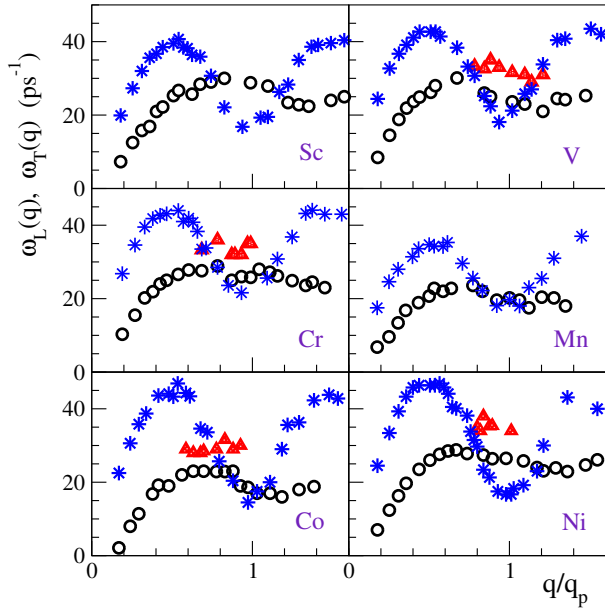
Figure 8. Dispersion relations for several metals. Stars: Longitudinal dispersion obtained from the AIMD results for the positions of the maxima in the spectra of the longitudinal current, $J_L(q,\omega)$. Open circles and triangles: Transverse dispersion from the positions of the peaks in the spectra $J_T(q,\omega)$.

Figure 9. Transverse current spectra, $J_T(q,\omega)$, at several q-values for l-Sc at $T = 1875$ K.
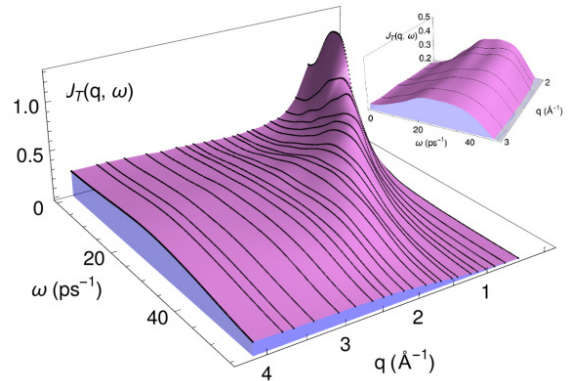
Figure 10. Same as the previous graph but for l-V at $T = 2173$ K. The inset gives a detailled view of the region where the $J_T(q,\omega)$ displays two maxima.
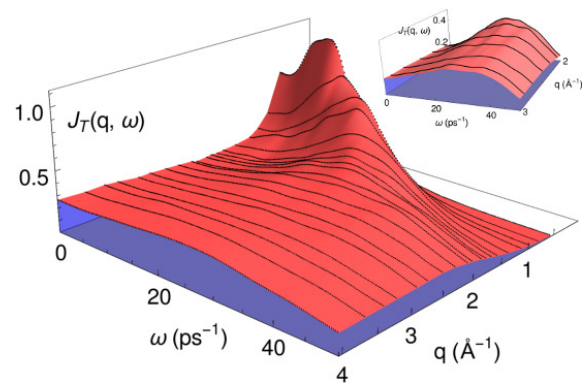
Figure 11. Same as the previous graph but for l-Cr at $T = 2173$ K.

the peak's frequency increases, reaches a maximum value at $q \approx (2/3)q_p$, and finally slowly decreases until the peaks disappear at $\approx 3.0q_p$. This can be observed in Figures 9-11 which represent the calculated $J_T(q,\omega)$ for l-Sc, l-V and l-Cr, as a function of ω, and for a range $0 < q \leq 4.2$ Å^{-1}.

Moreover, we have found that for some metals (l-V, l-Cr, l-Co and l-Ni) the corresponding $J_T(q,\omega)$ displayed, within a limited q-range, another, higher frequency, peak. Broadly speaking, those high-frequency peaks appeared in the q-region: $0.8 \leq q/q_p \leq 1.2$. For the other metals, (i.e. l-Sc, l-Ti, l-Mn and l-Fe) the results are not conclusive because, besides the lower frequency peak, we also found higher frequency shoulders instead of peaks.

At this point, we stress that the existence of another, high frequency branch, has already been found in some liquid metals at high pressure, i.e. Li, Na, Fe, Al and Pb, [2, 20, 21] and, more recently, also in l-Tl and l-Pb [19, 21] at ambient pressure. Although this has been considered as a feature more typical of liquid metals at high pressure, however the present results suggest that it is not so uncommon in liquid metals at ambient pressure.

From the AIMD results for the $J_T(q,t)$, we have also calculated [31, 32] the associated shear viscosity coefficient η, and the results are given in in Table 4.

4. Conclusions

An *ab initio* simulation method has been used to calculate several static and dynamic collective properties of some bulk liquid 3*d* transition metals at thermodynamic states near their respective melting points. To our knowledge, this is the first AIMD study performed to evaluate those properties in these metals.

The obtained results for the static structure, as characterized by static structure factor $S(q)$, show a good agreement with the available experimental data. A more detailed study of the liquid local structure, by using the Honeycutt-Andersen method, has shown a substantial presence of perfect and distorted icosahedral structures.

The power spectra of the velocity autocorrelation functions, $Z(\omega)$ has revealed a two peak structure (l-V and l-Co), a peak and a shoulder (l-Sc and l-Cr) and just a peak for l-Mn.

As for the dynamic properties, we have focused on the collective dynamics as described by the longitudinal and transverse currents. We have evaluated the associated spectral functions and the corresponding dispersion relations. For some metals, we have obtained two branches of transverse modes, with the high frequency branch appearing over a limited q-range which is always located in the second pseudo-Brillouin zone. Moreover, these results further support the idea [19] of a correlation between the existence of a second high frequency peak (or shoulder) in the $Z(\omega)$ and the emergence of a second, high frequency, branch of transverse modes.

Results have also been obtained for several transport coefficients such the self-diffusion, adiabatic sound velocity and shear viscosity. Whereas the calculated values for the adiabatic sound velocity show a reasonable agreement with the available experimental data, the lack of experimental data for the self-diffusion and the shear viscosity, provides, in our opinion, further relevance these results.

Acknowledgments

References

[1] del Rio B G, Rodríguez O, González L E and González D J 2017 *Comput. Mat. Sci.* **139** 243
[2] Marqués M, González L E and González D J 2015 *Phys. Rev. B* **92** 134203
Marqués M, González L E and González D J 2016 *J. Phys.: Condens. Matter* **28** 075101
[3] del Rio B G, González D J, González L E 2016 *Phys. of Fluids* **28** 107105
del Rio B G, González D J, González L E 2017 *J. Chem. Phys.* **146** 034501
[4] Waseda Y 1980 *The Structure of Non-Crystalline Materials*, McGraw-Hill, New York
[5] Schenk T, Holland-Moritz D, Simonet V, Bellissent R and Herlach D M 2002 *Phys. Rev. Lett.* **89** 075507
Inui M, Maruyama K, Kajihara Y and Nakada M 2009 *Phys. Rev. B* **80** 180201
[6] Lee G W, Gangopadhyay A K, Kelton K F, Hyers R W, Rathz T J, Rogers J R, Robinson D S 2004 *Phys. Rev. Letters* **93** 037802
Holland-Moritz D, Heinen O, Bellissent R, Schenk T 2007 *Mater. Sci. Eng. A* **449-451** 42
[7] Lee G W, Gangopadhyay A K, Hyers R W, Rathz T J, Rogers J R, Robinson D S, Goldman A I and Kelton K F 2008 *Phys. Rev. B* **77** 184102
[8] Blairs S 2007 *Intern. Materials Reviews* **52** 321
Blairs S 2007 *Phys. Chem. Liq.* **45** 399
[9] Casas J, Keita N M, Steinemann S G 1984 *Phys. Chem. Liq.* **14** 155
[10] Assael M J, Kakosimos K, Banish R M, Brillo J, Egry I, Brooks R, Quested P N, Mills K C, Nagashima A, Sato Y and Wakeham W A 2006 *J. Phys. Chem. Ref. Data* **35** 285
[11] Egry I, 1993 *Scr. Metall. Mater.* **28** 1273
[12] Said A H, Sinn H, Alatas A, Burns C A, Price D L, Saboungi M L, Schirmacher W 2006 *Phys. Rev B* **74** 172202
Horbach J, Rozas R E, Unruh T, Meyer A 2009 *Phys. Rev. B* **80** 212203
[13] Hosokawa S, Inui M, Matsuda K, Ishikawa D, and Baron A Q R 2008 *Phys. Rev. B* **77** 174203
[14] Johnson M W, McCoy B, March N H and Page D I 1977 *Phys. Chem. Liq.* **6** 243
Bermejo F J, Saboungi M L, Price D L, Alvarez M, Roessli B, Cabrillo C and Ivanov A 2000 *Phys. Rev. Letters* **85** 106
Chathoth S M, Meyer A, Koza M M and Juranyi F 2005 *Appl. Phys. Lett.* **85** 5003
[15] Todd J R and Brown J S 1976 *Phys. Lett A* **59** 302
[16] Hausleitner C, Kahl G and Hafner J 1991 *J. Phys.: Cond. Matter* **3** 1589
[17] Bhuiyan G M, Bretonnet J L, González L E and M. Silbert M 1992 *J. Phys.: Condens. Matter* **4** 7651
Bhuiyan G M, Silbert M and Stott M J 1996 *Phys. Rev B* **53** 636
[18] Rosenfeld Y 1986 *J Stat. Phys.* **42** 437
González D J, Ng D A and Silbert M 1990 *J. Non-Cryst. Solids* **117** 469
[19] Bryk T, Demchuk T, Jakse N and Wax J F 2018 *Frontiers in Physics* **6** 00006
[20] Bryk T, Ruocco G, Scopigno T and Seitsonen A P 2015 *J. Chem. Phys.* **143** 104502
[21] Bryk T, Demchuk T and Jakse N 2019 *Phys. Rev. B* **99** 014201
Bryk T and Jakse N 2019 *J. Chem. Phys.* **151** 034506
[22] del Rio B G and González L E 2017 *Phys. Rev. B* **95** 224201
[23] Gianozzi P *et al* 2009 *J. Phys.: Condens. Matter* **21**, 395502
Gianozzi P *et al* 2017 *J. Phys.: Condens. Matter* **29**, 465901
[24] Hohenberg P and Kohn W 1964 *Phys. Rev.* **136** B864
Kohn W and Sham L J 1965 *Phys. Rev.* **140** A1133
[25] Perdew J P, Burke K and Ernzerhof M 1996 *Phys. Rev. Letters* **77** 3865
[26] Vanderbilt D 1990 *Phys. Rev. B* **41** 7892
[27] Calderín L, González L E and González D J 2009 *J. Chem. Phys.* **130** 194505
Calderín L, González L E and González D J 2011 *J. Phys.: Cond. Matter* **23** 375105
Calderín L, González L E and González D J 2013 *J. Phys.:*

Cond. Matter **25** 065102

[28] J. D. Honeycutt J D and Andersen H C 1987 *J. Phys. Chem.* **91** 4950
Clarke A S and Jonsson H 1993 *Phys. Rev. B* **47** 3975
Luo W K , Sheng H W , Alamgir F M, Bai J M, He J H and Ma E 2004 *Phys. Rev. Letters* **92** 145502

[29] Marcus Y 2017 *Chem. Thermody.* **109** 11

[30] Balucani U and Zoppi M 1994 *Dynamics of the Liquid State*, (Oxford: Clarendon)

[31] González D J, González L E, López J M and Stott M J 2001 *J. Chem. Phys.* **115** 2373
González D J, González L E, López J M and Stott M J 2002 *Phys. Rev. B* **65** 184201

[32] Palmer B J 1994 *Phys. Rev. E* **49** 359
Balucani U, Brodholt J P, Jedlovszky P and Vallauri R 2000 *Phys. Rev. E* **62** 2971